ACS APPLIED MATERIALS & INTERFACES

Research Article

www.acsami.org

Near-Infrared Light-Triggered Drug-Delivery Vehicle for Mitochondria-Targeted Chemo-Photothermal Therapy

Enguo Ju,[†,‡] Zhenhua Li,[†,‡] Zhen Liu,[†,‡] Jinsong Ren,*[,†] and Xiaogang Qu*[,†]

[†]State Key Laboratory of Rare Earth Resource Utilization and Laboratory of Chemical Biology, Changchun Institute of Applied Chemistry, Chinese Academy of Sciences, Changchun 130022, People's Republic of China

[‡]Graduate School of the Chinese Academy of Sciences, Beijing 100039, People's Republic of China

Supporting Information

ABSTRACT: A novel drug-delivery vehicle for mitochondria-targeted chemo-photothermal therapy was demonstrated. A cytochrome *c*-specific binding aptamer was employed to make the mesoporous silica-encapsulated gold nanorods efficiently accumulate in the mitochondria of cancer cells. This nanocarrier can load various hydrophobic therapeutic agents acting on mitochondria to enhance the therapeutic efficiency and simultaneously depress the toxic side effects. In addition, near-IR treatment could induce cytochrome *c* release and initiation of the mitochondrial pathway of apoptosis. Importantly, this multifunctional platform could integrate targeting, light-triggered release, and chemo-photothermal therapy into one system. We hope that such a system could open the door to the fabrication of a multifunctional mitochondria-targeted drug-delivery vehicle for cancer therapy.

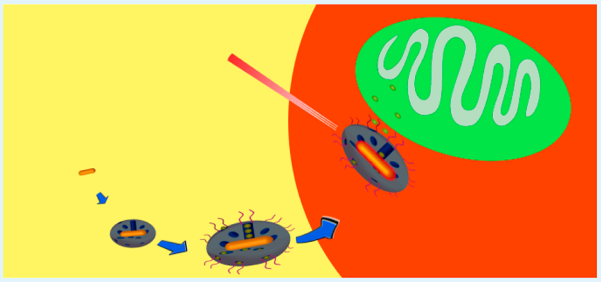

KEYWORDS: *aptamer, mitochondria, drug delivery, chemo-photothermal therapy*

1. INTRODUCTION

The advent of advanced molecular biology technology has conferred a deeper understanding of the mechanisms of diseases, which leads to the rational design of drugs working on specific sites within cells.[1] The molecular targets of many drugs are related to certain organelles inside mammalian cells. If drugs could be delivered specifically to the organelle of interests, such as anticancer drug doxorubicin to the nucleus or paclitaxel to the mitochondria, their therapeutic effect could be greatly enhanced.[2−4] However, it is insufficient to ensure the maximum utilization of drugs just by means of simple diffusion and random interaction. Therefore, organelle-targeted drug-delivery systems (DDSs) are highly desired because of the fact that they can improve the therapeutic efficiency and simultaneously depress the toxic side effects. Recently, mitochondria-targeted nanocarriers have attracted much attention because of the progressive evidence that mitochondrial dysfunction is responsible for a number of diseases including neurodegenerative and neuromuscular diseases, obesity and diabetes, ischemia-reperfusion injury, and cancer.[5,6] Mitochondria exert vital functions in physiological and pathological scenarios as well as energy production, which is essential for the survival of eukaryotic cells.[7] On the other hand, mitochondria are decisive regulators of the intrinsic pathway of apoptosis, which is regarded as the major mode of cell death in cancer therapy.[8] Because mitochondria play a pivotal role in cell death, a strategy based on mitochondria-targeted treatment represents a promising approach for cancer therapy. For instance, single-walled carbon nanotubes and bacterial magnetic nanoparticles were used to target mitochondria for cancer photothermal therapy.[9,10] When exposed to a 980-nm laser energy or external magnetic field, cells would receive an apoptotic stimulus, leading to mitochondrial depolarization, cytochrome *c* (Cyt *c*) release, and caspase activation. Also, surface modification of drug-loaded liposomes with various mitochondriotropic ligands, such as lipophilic cations, mitochondria-targeting signal peptides, and mitochondrial protein import machinery, showed significant improvement in drug action.[11−18] However, to the best of our knowledge, no study has yet been reported about the construction of a mitochondria-targeted light-triggered drug-delivery vehicle combining both chemotherapy and photothermal therapy.[19−22]

Herein, for the first time, we report an efficient mitochondria-targeted drug carrier based on aptamer-conjugated mesoporous silica-encapsulated gold nanorods (AuMPs) for chemo-photothermal therapy. Aptamers are single-stranded oligonucleotides that can act like antibodies and bind a wide array of biological targets with high affinity and specificity. With numerous advantages over antibodies, aptamers are easy to synthesize, are nonimmunogenic, and can be modified to resist denaturation and biodegradation.[23] Within the past few years, numerous studies have combined aptamer with nanomaterials and realized highly selective and efficient drug delivery.[24−26] Previously, Lau et al. reported a

Received: January 6, 2014
Accepted: February 24, 2014
Published: February 24, 2014

   dx.doi.org/10.1021/am5000883 | ACS Appl. Mater. Interfaces 2014, 6, 4364−4370

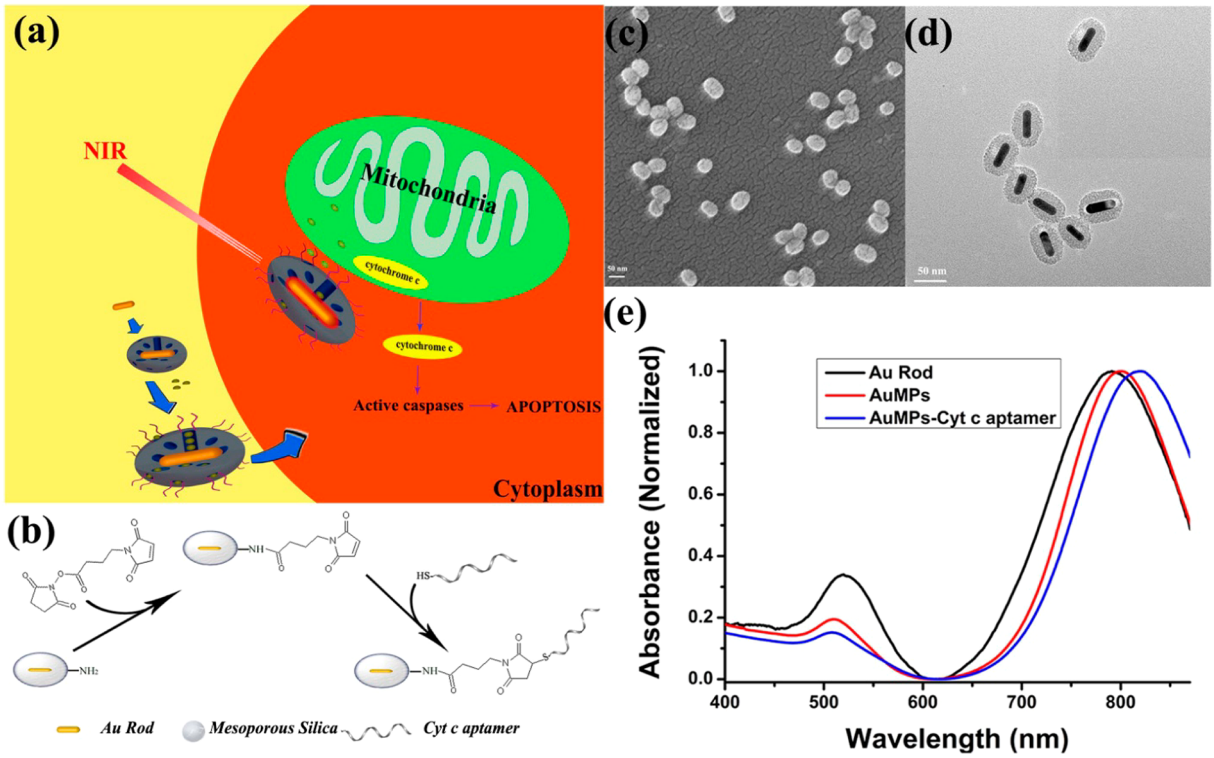

Figure 1. (a) Schematic illustration of the structure of the polyvalent aptamer-functionalized mesoporous silica-encapsulated AuMP-based nanocarriers and the targeted delivery of drug to the mitochondria of cancer cells. (b) Schematic illustration of the polyvalent modification procedure of the aptamer to the surface of AuMPs. (c) SEM and (d) TEM images of AuMPs. (e) UV/vis−NIR absorbance spectra of gold rods, AuMPs, and a AuMPs−Cyt c aptamer aqueous solution.

DNA aptamer that showed high specificity to Cyt *c* through systematic evolution of ligands by exponential enrichment (SELEX).[27] Cyt *c* is normally bound to the inner mitochondrial membrane by anionic phospholipid cardiolipin. We envisioned that, by taking the advantages of AuMPs and aptamers, the nanocarriers could target and deliver drug molecules directly into mitochondria of cancer cells. In addition, when a cell received an apoptotic stimulus from the heat produced by AuMPs under near-IR (NIR) light, Cyt *c* could be released into cytosol and it would trigger initiation of the mitochondrial pathway of apoptosis. The combination of mitochondria-targeted chemotherapy and photothermal therapy could improve the tumoricidal efficiency relative to the employment of each approach independently. Furthermore, NIR light could also stimulate drug release and enable the tunable release of the drug acting on mitochondria.

2. EXPERIMENTAL SECTION

2.1. Reagents and Materials. Tetrachloroauric acid ($HAuCl_4$), tetraethyl orthosilicate (TEOS), (3-aminopropyl)triethoxysilane (APTES), sodium borohydride ($NaBH_4$), ascorbic acid, silver nitrate ($AgNO_3$), and rotenone were obtained from Sigma-Aldrich. Cetyltrimethylammonium bromide (CTAB) and fluorescein isothiocyanate (FITC) were purchased from Alfa Aesar. All of the chemicals were used as received without further purification. Nanopure water (18.2 MΩ) was used in all experiments. Cyt *c*-specific binding aptamer used in this article was synthesized by Sangon Biotechnology (Shanghai, China). The sequence is designed as follows: 5′-CCG TGT CTG GGG CCG ACC GGC GCA TTG GGT ACG TTG TTG CTT TTT TTT-thiol-3′.

2.2. Preparation of AuMPs. First, $HAuCl_4$ (0.5 mM, 1.0 mL) and CTAB (0.2 M, 1.0 mL) were mixed together. Then, 0.12 mL of an ice-cold $NaBH_4$ aqueous solution (0.01 M) was added. A brownish-yellow solution was obtained as a seed solution kept at 25 °C at least 2 h before use. Next, CTAB (0.2 M, 100 mL), $AgNO_3$ (4 mM, 5.6 mL), $HAuCl_4$ (23 mM, 6.5 mL), and H_2O (95 mL) were mixed together, and ascorbic acid (0.08 M, 2.5 mL) was successively added to obtain a growth solution. Finally, 1.8 mL of the seed solution was mixed with the growth solution, and the solution was kept at room temperature for at least 6 h.

2.3. Preparation of Mesoporous Silica Coated AuMPs. The as-synthesized AuMPs were washed by centrifugation (75 mL aliquots at a time, 12000 rpm for 25 min). The residue was diluted to 50 mL by adding water. Then, NaOH (0.1 M, 500 μL) was added to adjust the pH of the solution. Following this step, three injections of 20% TEOS in methanol (150 μL) were added every 30 min, and the mixture was kept stirring for 6 h. CTAB was removed by refluxing in acidic methanol. To get amino-modified particles, 10 μL of APTES in 100 μL of methanol was added under stirring for another 5 h. As for fluorescein-labeled AuMPs, 1 mg of FITC was first reacted with 22 μL of APTES in 1 mL of ethanol for 2 h in the dark, and then 100 μL was added to the AuMP solution.

2.4. Cyt *c*-Specific Binding DNA Aptamer Conjugation. A heterobifunctional cross-linking reagent, *N*-(γ-maleimidobutyryloxy)-succinimide, was employed to functionalize AuMPs with aptamer. AuMPs (3 mg) were first suspended in a solution of a phosphate-buffered saline (PBS) buffer (100 mM PBS, 150 mM NaCl, pH 7.3) and *N*,*N*-dimethylformamide (DMF) (7:3) containing *N*-(γ-maleimidobutyryloxy)succinimide for 1 h. The resulting particles were centrifuged and washed with DMF twice. Before functionalization of the aptamer, we first incubated DNA (100 μM, 100 μL) with 50 μL of tris (2-carboxyethyl) phosphine (TCEP) to obtain free sulfhydryl groups. Then, the aptamer was mixed with maleimide-modified AuMPs in a PBS buffer (100 mM, 1 M NaCl, pH 7.3), and the solution was stirred at room temperature for 24 h. Finally, the nanoparticles were centrifuged and washed with a PBS buffer. All of the supernatant was collected for UV/vis absorbance measurement. Through calculation of the difference of absorbance at 260 nm

dx.doi.org/10.1021/am5000883 | ACS Appl. Mater. Interfaces 2014, 6, 4364−4370

between the DNA solution before and after reaction, the DNA immobilization efficiency was determined as 3 μmol/g AuMPs.

2.5. Drug-Loading and -Release Experiments. The AuMP nanoparticles (1 mg/mL) were incubated in dimethyl sulfoxide (DMSO) of rotenone (1 mg/mL) for 24 h followed by centrifugation and repeated washing with DMSO to remove the physisorption of rotenone. The washing solutions were collected, and the loading efficiency was calculated from the difference of the initial and final drugs. Rotenone-loaded AuMPs were then conjugated with aptamers as in the method mentioned above. Drug-release experiments were conducted as follows: a drug-loaded AuMPs−Cyt *c* aptamer complex was placed in a cuvette, and 10% ethanol was added. An excitation laser of 808 nm was exposed to excite the release of the drug. The absorption at 299 nm in the supernatant was determined for monitoring the release of the drug.

2.6. Apparatus and Characterizations. Fourier transform infrared (FT-IR) analyses were performed on a Bruker Vertex 70 FT-IR spectrometer. Scanning electron microscopy (SEM) images were recorded on a Hitachi S-4800 field-emission scanning electron microscope. Transmission electron microscopy (TEM) images were obtained with a FEI TECNAI G2 20 high-resolution transmission electron microscope operating at 200 kV. N_2 adsorption-desorption isotherms were recorded on a Micromeritics ASAP 2020M automated sorption analyzer. The specific surface areas were calculated from adsorption data in the low-pressure range using the Brunauer−Emmett−Teller model, and the pore size was determined following the Barrett−Joyner−Halenda method. Absorption spectra were measured on a Jasco V-550 UV/vis spectrometer. A continuous-wave diode laser (LSR808NL-2000) with a wavelength of 808 nm was used for the laser irradiation experiment.

2.7. Cell Culture. HeLa cells, human cervical cancer, were cultured in Dulbecco's modified Eagle's medium (DMEM) containing 10% (v/v) fetal bovine serum at 37 °C in a humidified atmosphere containing 5% (v/v) CO_2.

2.8. Cell Viability Assay. In vitro cytotoxicity was assessed by using 3-(4,5-dimethylthiazol-2-yl)-2,5-diphenyltetrazolium bromide (MTT) reduction assays. In a typical procedure, about 3000 cells were plated in 96-well plates for 24 h to allow the cells to attach and then incubated with nanoparticles. After incubation for 4 h, every well was washed two times with PBS. Fresh DMEM was then added to the wells. After NIR laser irradiation, the cells were incubated for 24 h. At the end of the incubation time, a MTT solution (5 mg/mL) was added to each well and the mixture was incubated for another 4 h. Finally, the incubation solution was removed, and DMSO (100 μL) was added. The absorbance of MTT was determined with Bio-Rad model 680 microplate reader at 490 nm (corrected for background absorbance at 630 nm).

2.9. Fluorescence Microscopy. HeLa cells were plated in 24-well culture plates. After 24 h, FITC−AuMPs and FITC−AuMPs−Cyt *c* aptamer complexes (50 μg/mL) were added to the cells, and the mixture was incubated for 2 or 4 h. After 2 times of washing with PBS, MitoTracker Red CMXRos (Invitrogen, USA) or LysoTracker (Invitrogen, USA) was used for staining for 15 min. The cells were then washed twice with PBS, and pictures were taken with an Olympus digital camera.

3. RESULTS AND DISCUSSION

As shown in Figure 1a, we first synthesized AuMPs and subsequently coated the nanoparticles with a mesoporous silica layer.[28−33] To functionalize the AuMPs with Cyt *c* aptamer, AuMPs were modified with amine groups through reaction with APTES (Figure 1b). The amine-modified AuMPs were then reacted with a heterobifunctional cross-linking reagent to obtain maleimide-terminated AuMPs. A AuMPs−Cyt *c* aptamer complex was finally synthesized through conjugation between maleimide-terminated AuMPs with a 3-thiol-modified aptamer. SEM and TEM showed that the AuMPs were homogeneously and individually coated by a mesoporous silica shell (Figure 1c,d). The silica shell was estimated to have a homogeneous thickness of ∼20 nm and was composed of disordered mesopores, offering an opportunity for AuMPs to be employed as a general drug carrier (Figure S1 in the Supporting Information, SI). The successful conjugation of aptamer onto AuMPs was proved by a decrease of absorbance of DNA (260 nm) in the supernatant (Figure S2 in the SI), which was also verified by the appearance of the characteristic asymmetric stretching mode of the imidyl group (1733 cm^{-1}) and the amide vibrations (1570 cm^{-1}) (Figure S3 in the SI). The optical properties of gold rods, AuMPs, and AuMPs−Cyt *c* aptamer were studied by UV/vis spectra (Figure 1e). All spectra possessed two absorption bands. The band at 510 nm corresponded to a transverse plasmon resonance, and the other at around 800 nm represented a longitudinal plasmon resonance. To demonstrate the potential of a AuMPs−Cyt *c* aptamer complex for photothermal cancer therapy, we carried out a control experiment by exposing aqueous solutions of AuMPs−Cyt *c* aptamer to NIR laser irradiation at 808 nm with different power densities. As shown in Figure S4 in the SI, the temperature increased monotonically with the radiant energy, indicating that the nanocarrier could be irradiated by the NIR light, which could potentially provide deep-tissue penetration with high spatial precision.

To evidence the decisive role of the conjugated Cyt *c* aptamer in the mitochondria localization, fluorescein isothiocyanate was attached to AuMPs to make the NPs have bioimaging functionality. Then, AuMPs and a AuMPs−Cyt *c* aptamer complex were incubated with HeLa cells for 4 h, and its subcellular locations were observed. As shown in Figure 2, AuMPs that were not functionalized with the Cyt *c* aptamer randomly distributed inside the cells, with no particular mitochondrial localization. In contrast, most of the internalized AuMPs−Cyt *c* aptamer complex was colocalized with mitochondria (yellow color), indicating that the internalized AuMPs−Cyt *c* aptamer complex was effectively and specifically

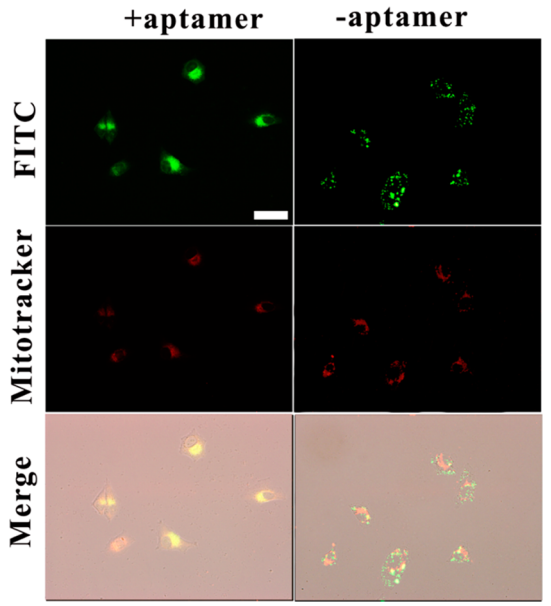

Figure 2. Specific targeting of the FITC−AuMPs−Cyt *c* aptamer complex to mitochondria inside HeLa cells. The mitochondria of the cells were stained with Mitotracker Red CMXRos. Scale bar equals 50 μm.

dx.doi.org/10.1021/am5000883 | ACS Appl. Mater. Interfaces 2014, 6, 4364−4370

targeted to the mitochondria. It can be concluded that the Cyt *c* aptamer was an indispensable medium for interacting with Cyt *c* and realizing mitochondria targeting. We also incubated nanoparticles with cells with 1 and 4 h, followed by incubating with red fluorescent lysotracker to stain the lysosomal compartments. As shown in Figure 3, the fluorescence of

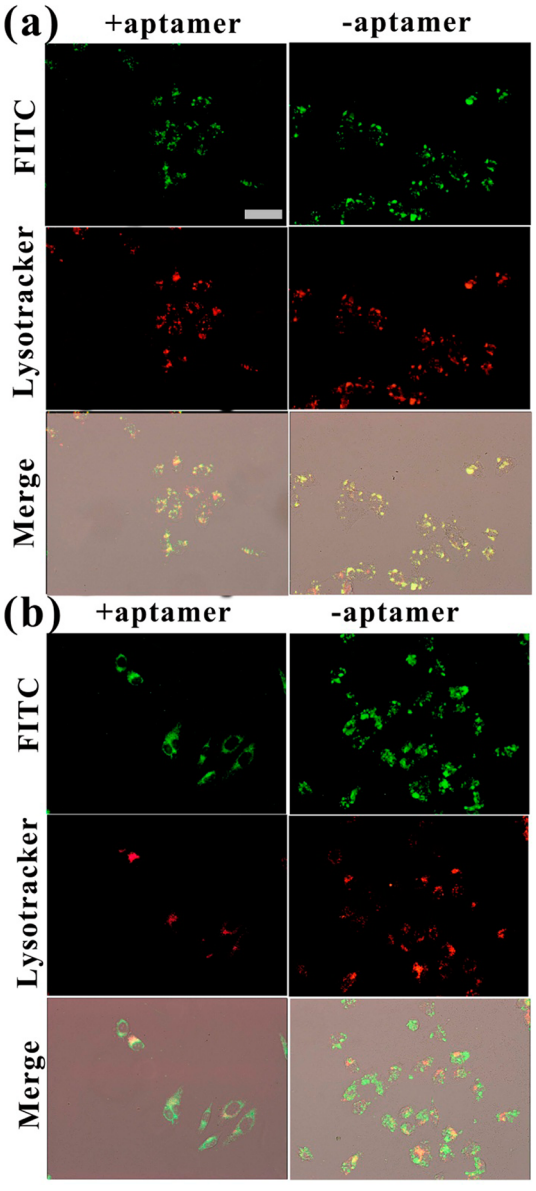

Figure 3. Spatial distributions of AuMPs and the AuMPs−Cyt *c* aptamer in HeLa cells. Cells were incubated with nanoparticles (a) for 1 h and (b) for 4 h. Lysosomes were stained by Lysotracker Red. Scale bar equals 50 μm.

both AuMPs and the AuMPs−Cyt *c* aptamer complex was colocalized with lysotracker within 1 h, whereas after 4 h of incubation, nanoparticles were found to be escaping from the lysosome. These observations could be explained based on the surface charge reversal that negatively nanoparticles undergo because of the transfer of protons from the bulk solution to the surface of the nanoparticles under acidic conditions, better known as the "proton sponge effect".[34,35] Combined with Figures 2 and 3, we concluded that the AuMPs−Cyt *c* aptamer complex was first taken up in cells and translocated into lysosome, and then the nanoparticles escaped from lysosome. Through the binding action between Cyt *c* and aptamer, the nanoparticles were finally accumulated at the mitochondria.

As a direct test of mitochondria-targeted drug delivery of the AuMPs−Cyt *c* aptamer, rotenone, a specific inhibitor of mitochondrial electron transport complex I, was chosen as a proof-of-principle drug in this study. Rotenone could induce apoptosis although the generation of reactive oxygen species as well as the activation of c-*jun* N-terminal kinase and p38 mitogen-activated protein kinases.[36] The drug loading was accomplished by soaking the AuMPs−Cyt *c* aptamer in a solution of 1 mg/mL rotenone of DMSO. The loading percentage by weight of rotenone in the AuMPs−Cyt *c* aptamer was calculated to be 7.3%. Next, we investigated the release kinetics of the rotenone-loaded AuMPs−Cyt *c* aptamer (Rot@AuMPs−Cyt *c* aptamer). It should be mentioned that the photothermal effect of AuMPs that we employed here played two vital roles. First, the stimulus of heat made Cyt *c* release into the cytosol from the mitochondria, and it triggered programmed cell death through apoptosis, which can be used for cancer therapy. Second, this photothermal effect could also stimulate drug release. As shown in Figure 4, a control

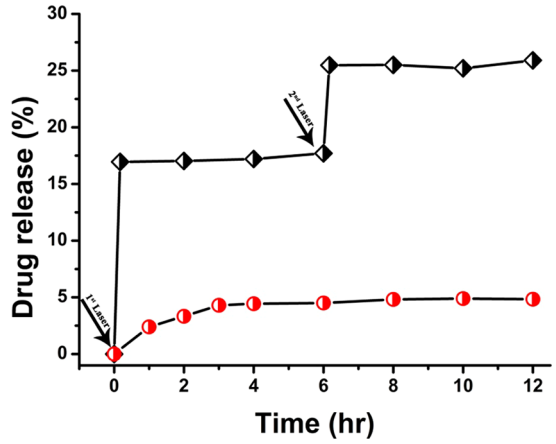

Figure 4. Rotenone release profile in the Rot@AuMPs−Cyt *c* aptamer complex with and without laser irradiation (808 nm, 2 W/cm^2, 10 min).

experiment was first carried out to display that the model drug did not exhibit a significant release. However, an obvious increase in the amount of drug release was observed after NIR irradiation, and the drug molecules in the pores exactly followed the signal switching from burst to slow release for each operation. The release of the drug was due to the absorption of NIR irradiation, which quickly heated the nanoparticles, resulting in acceleration of desorption and release of the rotenone hosted on the nanoparticle pores. At the same time, the heating of the surrounding fluid decreases its viscosity, favoring diffusion of the drug away from the nanoshells. However, the second NIR irradiation could only cause 7% drug release, while the first irradiation led to nearly 17% drug release. We speculated that this phenomenon was caused by the low photostability of AuMPs. That is, the NIR absorbance peak of the AuMPs would diminish after a period of laser irradiation due to the "melting effect". As a result, the photothermal conversion efficiency would decrease, which leads to a decreased drug release upon the second irradiation. The

dx.doi.org/10.1021/am5000883 | ACS Appl. Mater. Interfaces 2014, 6, 4364−4370

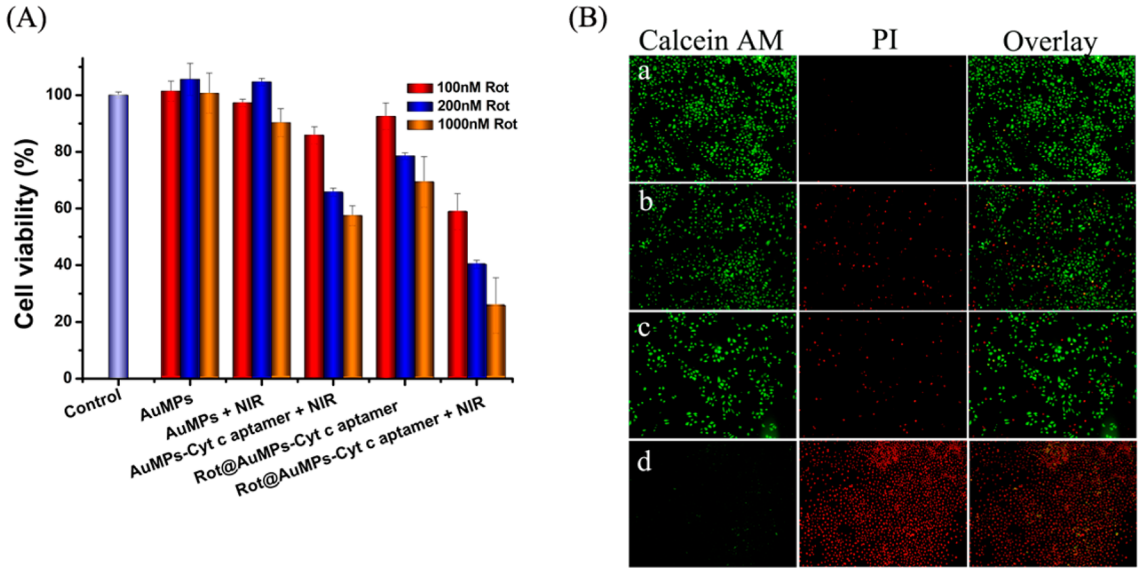

Figure 5. (A) Cytotoxicity assays of HeLa cells treated with AuMPs, the AuMPs−Cyt *c* aptamer, the Rot@AuMPs−Cyt *c* aptamer and those upon 808-nm laser irradiation with a power density of 1.5 W/cm^2 for 5 min. (B) Fluorescence microscopy images of HeLa cells incubated with (a) AuMPs with NIR irradiation, (b) the AuMPs−Cyt *c* aptamer with NIR irradiation, (c) the Rot@AuMPs−Cyt *c* aptamer without NIR irradiation, and (d) the Rot@AuMPs−Cyt *c* aptamer with NIR irradiation. Viable cells were stained green with calcein AM, and dead cells were stained red with PI.

above indicated that the AuMPs−Cyt *c* aptamer complex was one kind of effective NIR laser-triggered drug-release vehicle.

To demonstrate enhancement of the anticancer efficiency of the Rot@AuMPs−Cyt *c* aptamer DDSs, the cytotoxicity of the carriers was first measured by in vitro MTT assay (Figure S5 in the SI). The cell viability of HeLa cells remained above 80% when they were treated with AuMPs up to a concentration of 500 μg/mL for 24 h. This is consistent with the previous finding that silica is not intrinsically toxic. In this study, we chose a low power density of the laser to avoid killing cancer cells directly through the hyperthermic effect. As shown in Figure 5A, no obvious cytotoxicity was observed when cells were incubated with AuMPs in the presence of NIR irradiation. However, the viability of cells treated with the mitochondria-targeted AuMPs−Cyt *c* aptamer complex reduced significantly under the condition of NIR irradiation. This phenomenon may be attributed to the direct mitochondrial damage in the presence of thermally sensitive AuMPs−Cyt *c* aptamer. A previous study has confirmed that death was induced by cell apoptosis through detection of Cyt *c* release and subsequent caspase 3 activation.[9] In the presence of laser irradiation, the photothermal convention materials could efficiently convert the laser energy into heat and selectively destroy mitochondria, inducing mitochondrial depolarization, Cyt *c* release, and initiation of the mitochondrial pathway of apoptosis to activate caspase. After loading of the drug, the Rot@AuMPs−Cyt *c* aptamer exhibited low toxicity due to the leakage of a slight amount of rotenone from the pores. After NIR irradiation, the cell viability decreased significantly. This was lower than chemotherapy or photothermal therapy alone, suggesting that chemo-photothermal therapy of the rotenone-loaded AuMPs−Cyt *c* aptamer complex demonstrated a synergistic effect. Moreover, rotenone could be released fast from the carriers after NIR laser irradiation, which meant that the NIR light acted as a trigger to induce the release of drugs and cause subsequent cell damage. This synergistic effect was further confirmed by Live-Dead assay. As shown in Figure 5B, compared with chemo- and photothermal treatment alone, the combined treatment yielded higher cytotoxicity. Besides, targeting the chemotherapeutic drugs toward the mitochondria of cancer cells showed an enhanced therapeutic effect, which could lower the cytotoxic drug dosage requirements. Furthermore, because light could be manipulated precisely, the AuMPs−Cyt *c* aptamer complex provided a platform to deliver anticancer agents with exact control of the area, time, and dosage.

4. CONCLUSIONS

In conclusion, a novel drug-delivery vehicle for mitochondria-targeted chemo-photothermal therapy was demonstrated for the first time. A Cyt *c*-specific binding aptamer was employed to make the AuMPs efficiently accumulate in the mitochondria of cancer cells. This nanocarrier can load various hydrophobic therapeutic agents acting on mitochondria to enhance the therapeutic efficiency and simultaneously depress the toxic side effects. In addition, NIR treatment could induce Cyt *c* release and initiation of the mitochondrial pathway of apoptosis. Importantly, this multifunctional platform could integrate targeting, light-triggered release, and chemo-photothermal therapy into one system. We hope that such DDSs could open the door for the fabrication of a multifunctional mitochondria-targeted drug-delivery platform for cancer therapy.

■ ASSOCIATED CONTENT

Ⓢ Supporting Information

N_2 adsorption−desorption isotherms, UV/vis and FT-IR spectra, plots of temperature increase, cell viability, chemical structure, and a standard linear calibration curve of rotenone. This material is available free of charge via the Internet at http://pubs.acs.org.

■ AUTHOR INFORMATION

Corresponding Authors

*E-mail: jren@ciac.ac.cn.
*E-mail: xqu@ciac.ac.cn.

Notes

The authors declare no competing financial interest.

■ ACKNOWLEDGMENTS

We acknowledge financial support from the National Basic Research Program of China (Grants 2012CB720602 and 2011CB936004) and the National Natural Science Foundation of China (Grants 21210002, 91213302, and 21072182).

■ REFERENCES

(1) Torchilin, V. P. Recent Approaches to Intracellular Delivery of Drugs and DNA and Organelle Targeting. *Annu. Rev. Biomed. Eng.* **2006**, *8*, 343−75.
(2) Pathania, D.; Millard, M.; Neamati, N. Opportunities in Discovery and Delivery of Anticancer Drugs Targeting Mitochondria and Cancer Cell Metabolism. *Adv. Drug Delivery Rev.* **2009**, *61*, 1250−1275.
(3) Pan, L.; He, Q.; Liu, J.; Chen, Y.; Ma, M.; Zhang, L.; Shi, J. Nuclear-Targeted Drug Delivery of TAT Peptide-Conjugated Monodisperse Mesoporous Silica Nanoparticles. *J. Am. Chem. Soc.* **2012**, *134*, 5722−5725.
(4) Yuan, H.; Fales, A. M.; Vo-Dinh, T. TAT Peptide-Functionalized Gold Nanostars: Enhanced Intracellular Delivery and Efficient NIR Photothermal Therapy Using Ultralow Irradiance. *J. Am. Chem. Soc.* **2012**, *134*, 11358−11361.
(5) Wallace, D. C. The Mitochondrial Genome in Human Adaptive Radiation and Disease: on the Road to Therapeutics and Performance Enhancement. *Gene* **2005**, *354*, 169−180.
(6) Chan, D. C. Mitochondria: Dynamic Organelles in Disease, Aging, and Development. *Cell* **2006**, *125*, 1241−1252.
(7) Galluzzi, L.; Joza, N.; Tasdemir, E.; Maiuri, M. C.; Hengartner, M.; Abrams, J. M.; Tavernarakis, N.; Penninger, J.; Madeo, F.; Kroemer, G. No Death Without Life: Vital Functions of Apoptotic Effectors. *Cell Death Differ.* **2008**, *15*, 1113−1123.
(8) Kroemer, G.; Galluzzi, L.; Brenner, C. Mitochondrial Membrane Permeabilization in Cell Death. *Physiol. Rev.* **2007**, *87*, 99−163.
(9) Zhou, F.; Wu, S.; Wu, B.; Chen, W. R.; Xing, D. Mitochondria-Targeting Single-Walled Carbon Nanotubes for Cancer Photothermal Therapy. *Small* **2011**, *7*, 2727−2735.
(10) Choi, J.; Shin, J.; Lee, J.; Cha, M. Magnetic Response of Mitochondria-Targeted Cancer Cells with Bacterial Magnetic Nanoparticles. *Chem. Commun.* **2012**, *48*, 7474−7476.
(11) Boddapati, S. V.; D'Souza, G. G.; Erdogan, S.; Torchilin, V. P.; Weissig, V. Organelle-Targeted Nanocarriers: Specific Delivery of Liposomal Ceramide to Mitochondria Enhances Its Cytotoxicity in Vitro and in Vivo. *Nano Lett.* **2008**, *8*, 2559−2563.
(12) Del Gaizo, V. A. Novel TAT−Mitochondrial Signal Sequence Fusion Protein is Processed, Stays in Mitochondria, and Crosses the Placenta. *Mol. Ther.* **2003**, *7*, 720−730.
(13) Biswas, S.; Dodwadkar, N. S.; Deshpande, P. P.; Torchilin, V. P. Liposomes Loaded with Paclitaxel and Modified with Novel Triphenylphosphonium−PEG−PE Conjugate Possess Low Toxicity, Target Mitochondria and Demonstrate Enhanced Antitumor Effects in Vitro and in Vivo. *J. Controlled Release* **2012**, *159*, 393−402.
(14) Mo, R.; Sun, Q.; Xue, J.; Li, N.; Li, W.; Zhang, C.; Ping, Q. Multistage pH-Responsive Liposomes for Mitochondrial-Targeted Anticancer Drug Delivery. *Adv. Mater.* **2012**, *24*, 3659−3665.
(15) Yao, H.-J.; Ju, R.-J.; Wang, X.-X.; Zhang, Y.; Li, R.-J.; Yu, Y.; Zhang, L.; Lu, W.-L. The Antitumor Efficacy of Functional Paclitaxel Nanomicelles in Treating Resistant Breast Cancers by Oral Delivery. *Biomaterials* **2011**, *32*, 3285−3302.
(16) Zhou, J.; Zhao, W.-Y.; Ma, X.; Ju, R.-J.; Li, X.-Y.; Li, N.; Sun, M.-G.; Shi, J.-F.; Zhang, C.-X.; Lu, W.-L. The Anticancer Efficacy of Paclitaxel Liposomes Modified with Mitochondrial Targeting Conjugate in Resistant Lung Cancer. *Biomaterials* **2013**, *34*, 3626−3638.
(17) Sharma, A.; Soliman, G. M.; Al-Hajaj, N.; Sharma, R.; Maysinger, D.; Kakkar, A. Design and Evaluation of Multifunctional Nanocarriers for Selective Delivery of Coenzyme Q10 to Mitochondria. *Biomacromolecules* **2012**, *13*, 239−252.
(18) Callahan, J.; Kopecek, J. Semitelechelic HPMA Copolymers Functionalized with Triphenylphosphonium as Drug Carriers for Membrane Transduction and Mitochondrial Localization. *Biomacromolecules* **2006**, *7*, 2347−2356.
(19) Zhong, Y.; Wang, C.; Cheng, L.; Meng, F.; Zhong, Z.; Liu, Z. Gold Nanorod-Cored Biodegradable Micelles as a Robust and Remotely Controllable Doxorubicin Release System for Potent Inhibition of Drug-Sensitive and -Resistant Cancer Cells. *Biomacromolecules* **2013**, *14*, 2411−2419.
(20) Wang, C.; Xu, H.; Liang, C.; Liu, Y.; Li, Z.; Yang, G.; Cheng, L.; Li, Y.; Liu, Z. Iron Oxide@Polypyrrole Nanoparticles as a Multifunctional Drug Carrier for Remotely Controlled Cancer Therapy with Synergistic Antitumor Effect. *ACS Nano* **2013**, *7*, 6782−6795.
(21) Yang, K.; Wan, J.; Zhang, S.; Tian, B.; Zhang, Y.; Liu, Z. The Influence of Surface Chemistry and Size of Nanoscale Graphene Oxide on Photothermal Therapy of Cancer Using Ultra-Low Laser Power. *Biomaterials* **2012**, *33*, 2206−2214.
(22) Liu, X.; Tao, H.; Yang, K.; Zhang, S.; Lee, S.-T.; Liu, Z. Optimization of Surface Chemistry on Single-Walled Carbon Nanotubes for in Vivo Photothermal Ablation of Tumors. *Biomaterials* **2011**, *32*, 144−151.
(23) Wu, Y.; Sefah, K.; Liu, H.; Wang, R.; Tan, W. DNA Aptamer-Micelle as an Efficient Detection/Delivery Vehicle toward Cancer Cells. *Proc. Natl. Acad. Sci. U. S. A.* **2010**, *107*, 5−10.
(24) Xing, H.; Wong, N. Y.; Xiang, Y.; Lu, Y. DNA Aptamer Functionalized Nanomaterials for Intracellular Analysis, Cancer Cell Imaging and Drug Delivery. *Curr. Opin. Chem. Biol.* **2012**, *16*, 429−435.
(25) Zhu, G.; Ye, M.; Donovan, M. J.; Song, E.; Zhao, Z.; Tan, W. Nucleic Acid Aptamers: an Emerging Frontier in Cancer Therapy. *Chem. Commun.* **2012**, *48*, 10472−10480.
(26) Li, Z.; Liu, Z.; Yin, M.; Yang, X.; Yuan, Q.; Ren, J.; Qu, X. Aptamer-Capped Multifunctional Mesoporous Strontium Hydroxyapatite Nanovehicle for Cancer-Cell-Responsive Drug Delivery and Imaging. *Biomacromolecules* **2012**, *13*, 4257−4263.
(27) Lau, I. P. M.; Ngan, E. K. S.; Loo, J. F. C.; Suen, Y. K.; Ho, H. P.; Kong, S. K. Aptamer-Based Bio-Barcode Assay for the Detection of Cytochrome-c Released from Apoptotic Cells. *Biochem. Biophys. Res. Commun.* **2010**, *395*, 560−564.
(28) Zhang, Z.; Wang, L.; Wang, J.; Jiang, X.; Li, X.; Hu, Z.; Ji, Y.; Wu, X.; Chen, C. Mesoporous Silica-Coated Gold Nanorods as a Light-Mediated Multifunctional Theranostic Platform for Cancer Treatment. *Adv. Mater.* **2012**, *24*, 1418−1423.
(29) Yang, X.; Liu, X.; Liu, Z.; Pu, F.; Ren, J.; Qu, X. Near-Infrared Light-Triggered, Targeted Drug Delivery to Cancer Cells by Aptamer Gated Nanovehicles. *Adv. Mater.* **2012**, *24*, 2890−2895.
(30) Chang, Y.-T.; Liao, P.-Y.; Sheu, H.-S.; Tseng, Y.-J.; Cheng, F.-Y.; Yeh, C.-S. Near-Infrared Light-Responsive Intracellular Drug and siRNA Release Using Au Nanoensembles with Oligonucleotide-Capped Silica Shell. *Adv. Mater.* **2012**, *24*, 3309−3314.
(31) Jiang, Z.; Dong, B.; Chen, B.; Wang, J.; Xu, L.; Zhang, S.; Song, H. Multifunctional Au@mSiO$_2$/Rhodamine B Isothiocyanate Nanocomposites: Cell Imaging, Photocontrolled Drug Release, and Photothermal Therapy for Cancer Cells. *Small* **2012**, *9*, 604−612.
(32) Li, N.; Yu, Z.; Pan, W.; Han, Y.; Zhang, T.; Tang, B. A Near-Infrared Light-Triggered Nanocarrier with Reversible DNA Valves for Intracellular Controlled Release. *Adv. Funct. Mater.* **2012**, *23*, 2255−2262.
(33) Shen, S.; Tang, H.; Zhang, X.; Ren, J.; Pang, Z.; Wang, D.; Gao, H.; Qian, Y.; Jiang, X.; Yang, W. Targeting Mesoporous Silica-Encapsulated Gold Nanorods for Chemo-Photothermal Therapy with Near-Infrared Radiation. *Biomaterials* **2013**, *34*, 3150−3158.
(34) Slowing, I.; Trewyn, B. G.; Lin, V. S. Effect of Surface Functionalization of MCM-41-Type Mesoporous Silica Nanoparticles on the Endocytosis by Human Cancer Cells. *J. Am. Chem. Soc.* **2006**, *128*, 14792−14793.

(35) Vivero-Escoto, J. L.; Slowing, I. I.; Trewyn, B. G.; Lin, V. S. Mesoporous Silica Nanoparticles for Intracellular Controlled Drug Delivery. *Small* **2010**, *6*, 1952−1967.
(36) Deng, Y. T.; Huang, H. C.; Lin, J. K. Rotenone Induces Apoptosis in MCF-7 Human Breast Cancer Cell-Mediated ROS Through JNK and p38 Signaling. *Mol. Carcinog.* **2010**, *49*, 141−151.